Journal of Colloid and Interface Science **230,** 29–40 (2000)
doi:10.1006/jcis.2000.7019, available online at http://www.idealibrary.com on IDEAL®

Transient Surface Tension of an Expanding Liquid Sheet

Philippe Marmottant,* Emmanuel Villermaux,†,[1] and Christophe Clanet†

*LEGI–CNRS, Institut de Mécanique de Grenoble, BP 53X, 38041 Grenoble Cedex, France; and †IRPHE, UMR 6594, CNRS, Universités d'Aix-Marseille I and II, Campus de Saint Jérome, Service 252, 13397 Marseille Cedex 20, France

Received August 24, 1999; accepted June 5, 2000

We address the problem of dynamic surface tension using measurements of sheet diameters that results from the impact of a liquid jet of diameter d_0 on a small disk of diameter d_i ($d_i/d_0 \simeq 4$). At low velocities, the sheet diameter D is related to d_0 by the Weber number We, constructed with the liquid density ρ, the jet velocity u_0, and the surface tension σ at the rim: $D/d_0 = \frac{1}{8}We = \frac{1}{8}[\rho u_0^2/(\sigma/d_0)]$. This relation expresses the equilibrium between inertial forces and surface tension forces at the sheet rim. When a surfactant has been dissolved in the bulk of the liquid prior to the formation of the initial jet, the rim surface tension, and therefore the sheet diameter, depends on the amount of surfactant adsorbed at the rim. This amount is fixed by a competition between surface formation induced by radial extension and repopulation of the liquid interface in surfactant. The experimental setup proposed here provides a method to measure dynamic surface tension from sheet diameter measurements and symmetrically to monitor the adsorption of a surfactant on a liquid surface. The available adsorption time ranges from 10 to 100 ms. Experimental data obtained with two surfactants are in agreement with a model of a diffusion-controlled adsorption at the interface.

Key Words: **adsorption kinetics; dynamic surface tension; expanded film; stretched interface.**

1. INTRODUCTION

Dupré (1) first noticed that the surface tension of a water solution of soap just after formation is higher than at equilibrium. This is explained by the fact that the adsorption of the surfactant molecules diluted in the bulk of the liquid at the interface is not instantaneous. At the time of its creation, the interface is clear from surfactant and has the surface tension of the pure liquid. As time elapses, the concentration of surfactant increases at the interface up to an equilibrium value which sets the surface tension of the fully saturated interface.

To measure dynamic surface tension, Rayleigh proposed in 1869 the use of a jet with an elliptic section at the outlet (2). The wavelength of the oscillating section of the jet in space is a function of surface tension, allowing, under usual laboratory conditions, one to follow its evolution in time for a time interval of the order of 30 ms.

Bond studied in 1937 the impact of two opposed jets (3), resulting in a thin axisymmetrical sheet. The sheet diameter depends on the surface tension at its rim. This provides another simple method to measure surface tension. We propose here to follow this method in a similar configuration described below.

Bond's interpretation of his measurements were biased by a flawed analysis, as pointed out by Ward and Tordai (4). The correct solution of the diffusion equations, accounting for the reversibility of the adsorption process at the interface, was given by these authors for diffusion processes (4). Measurements conducted with alcohols of different chain length are well accounted for by Ward and Tordai's law (5, 6). However, diffusion is not the only ingredient involved in the repopulation process of the liquid surface by surfactant molecules. The transfer of surfactant molecules from the bulk just below the surface and the interface is the second step which follows diffusion. This step can be, depending on the surfactant, the limiting step of the adsorption kinetics. For instance, oscillating jet measurements with 1,9-nonanediol (7) show an adsorption entirely controlled by the transfer of surfactant from the volume to the surface. Both effects, diffusion and transfer, should thus be accounted for in a comprehensive study of the problem. In practice, however, one of the two processes is often much slower than the other.

A liquid jet impacting at the center of a small disk is deflected radially in the form of a thin liquid sheet, as first described by Savart in 1833 (8). A cylindrical liquid element before the impact is thus stretched, its surface to volume ratio increasing linearly with radial distance continuously up to the rim of the sheet. The diameter of the sheet is determined by the liquid surface tension at the rim, whose value results from the competition between surface creation and adsorption kinetics of the dissolved surfactant.

We present in this paper a complete investigation of this configuration, using several injection diameters and surfactants, some of them having a known adsorption kinetics. This method allows the determination of adsorption times ranging from 10 to 100 ms.

2. EXPERIMENTAL SETUP

The experimental setup has been designed to produce a constantly renewed stretched liquid sheet (Fig. 1). It consists in the

[1] To whom correspondence should be addressed. Fax: 33-491 635261. E-mail: villerma@lrc.univ-mrs.fr.

0021-9797/00 $35.00

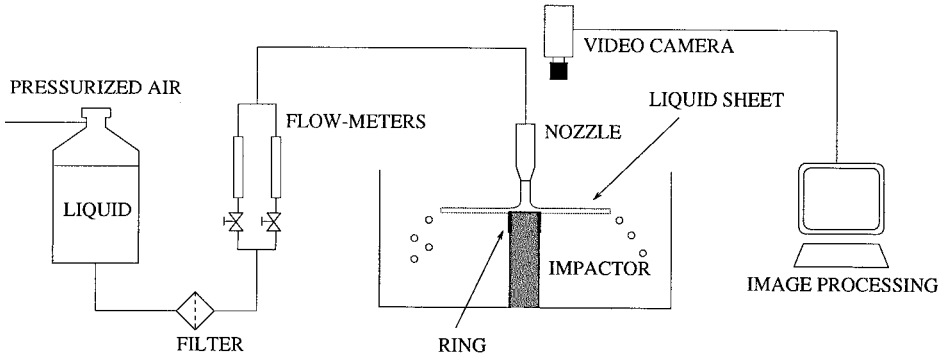

FIG. 1. Experimental setup.

impact of a cylindrical jet vertically on a disk. The jet is produced by a convergent nozzle to restrain turbulence at the nozzle exit. The liquid velocity is set by calibrated precision flow meters.

After the impact, the liquid spreads out radially and produces a thin circular sheet of liquid. When impacting right at the center of the disk, the sheet is axisymmetrical. The sheet is projected in the form of a cone whose top angle can be adjusted with a cylindrical ring (Fig. 2). As described by Savart (8), the shape of the sheet after impingement on a flat disk is a bell (see Fig. 3). The measurement of the surface tension at the rim of the sheet, which is our goal in this study, is more easily done when the sheet is flat and develops in the horizontal plane, with no radius of curvature. To realize this condition, the ring is positioned slightly above the surface of impingement, allowing adjustment of the angle of the sheet with the horizontal plane.

Several jet diameters were tested (measured at the injector's exit, after natural constriction): $d_0 = 0.8$, 2.8, 4.0, and 4.9 mm, with different impactors of respective diameters 3, 10.8, 10.8, and 20 mm. The liquid sheets were illuminated sideways and filmed by an analog Sony 8500 CE video camera (shutter speed 1/1000 s) located above the sheet. Images were digitalized with an 8-bit Neotech frame grabber card and analyzed with NIH Image software on which length measurements were manually performed. Because of the unsteadiness of the drop formation at the rim, an average of at least 20 instantaneous images was necessary to measure the sheet diameter D accurately (Fig. 4).

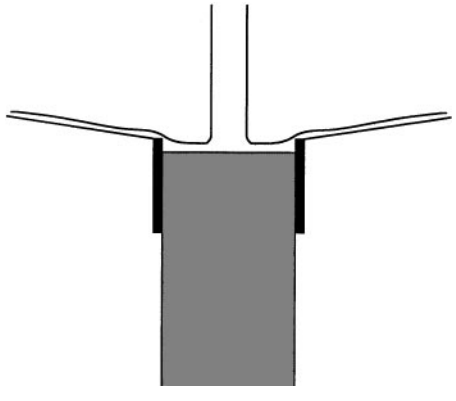

FIG. 2. The adjustable ring around the impactor bends the sheet up, keeping it on the horizontal surface.

3. EXPERIMENTAL RESULTS

3.1. Experiments with Water

We used tap water whose surface tension was found to be 70 mN/m within ± 2 mN/m of accuracy, as determined by the Harkins and Brown (9) drop weight technique, along with Wilkinson's experimental table (10). The drops were slowly formed in a saturated atmosphere before weighting. The sheet diameter measurements are displayed in Fig. 5 for different injector diameters.

The sheet diameter is proportional to the square of the velocity until a critical velocity, above which the diameter decreases (11). This second stage is due to the development of a shear instability with the surrounding air at rest. In this regime, the sheet oscillates like a flag and the rim breaks closer to the impactor center as u_0 is increased. Below the critical velocity, the sheet remains flat and its diameter is fixed by the surface tension forces at the edge as we will discuss in Section 4.

3.2. Experiments with Surfactants

A nonionic surfactant, octan-1-ol, was chosen because of the wide literature dedicated to its adsorption kinetics properties. The octan-1-ol we used had a purity grade of 99% (manufactured by Sigma).

In our attempts to change surface tension, we used several surfactants. An industrial detergent, Ajax, was used because of its high solubility. This surfactant, manufactured by Colgate-Palmolive Professional, is very soluble and easy to handle. We do not know its exact composition: global properties only will be measured. It is nevertheless a practibility test for our surface tension measurement device, even if its adsorption properties are subject to caution since it could contain ionic surfactant.

The surfactant was dissolved in 30 liters of water and stored in a tank. Pushed by pressurized air, the liquid flowed through the flow meters before exiting at the injector. The sheet diameter was then measured for different injection velocities. The results

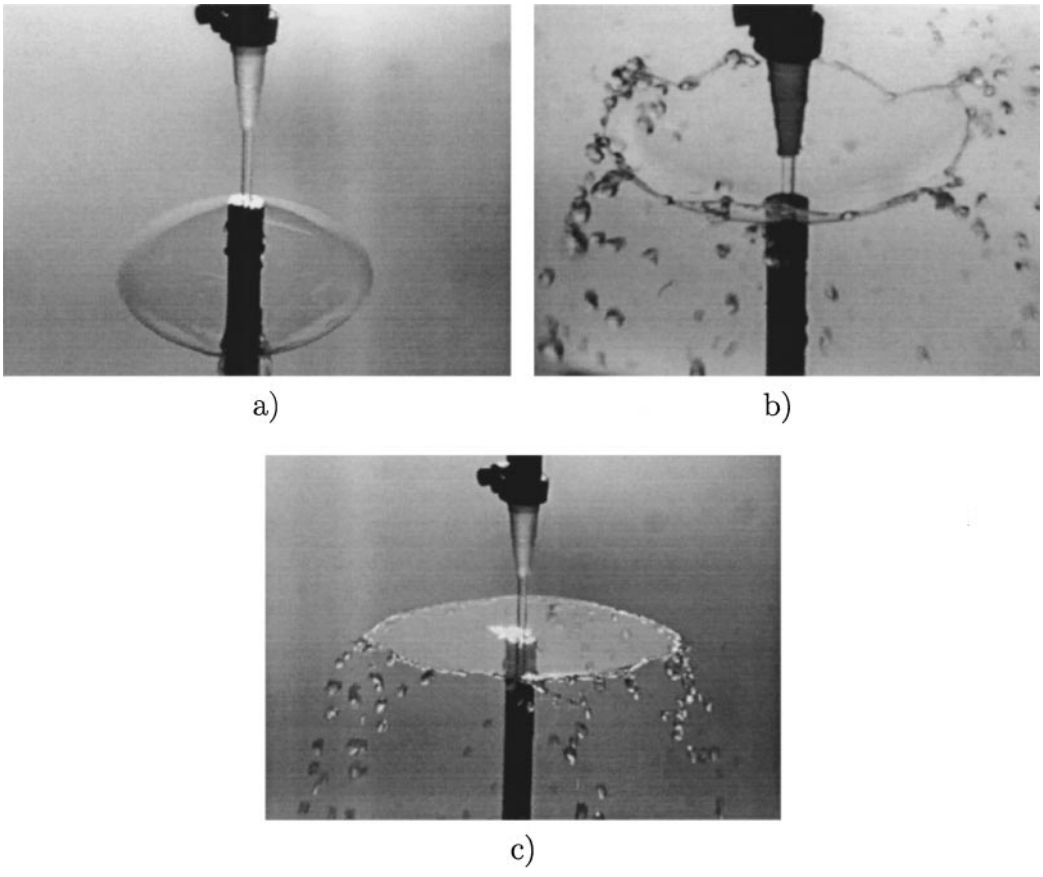

FIG. 3. Pictures of (a) a water bell shape, with the ring in the down position, (b) a cup, with the ring up, and (c) a plane sheet, with the ring slightly above the impingement surface.

obtained with two surfactant concentrations (Figs. 6 and 7) show that the diameter of a highly concentrated solution is proportional to the square of velocity but with a higher proportionality coefficient. On the other hand, for a lower concentration solution, the diameter is first close to the diameter determined with pure water and then rises toward the high-concentration curve. We observe a transition due to the gradual adsorption of surfactant on the surface, which lowers surface tension. As is shown in the next section, the sheet diameter is inversely proportional to the surface tension at the rim.

4. SHEET DIAMETER

4.1. Diameter in the Inviscid Limit

The liquid sheet ends with a toroidal rim whose radial position is fixed by the equilibrium between inertial forces and surface

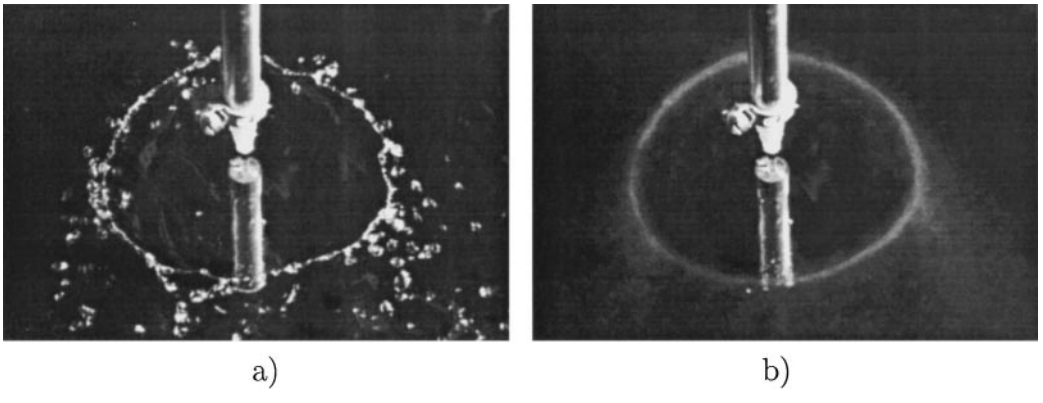

FIG. 4. (a) Instantaneous image of the liquid sheet; the rim is perturbed. (b) Average image of the sheet.

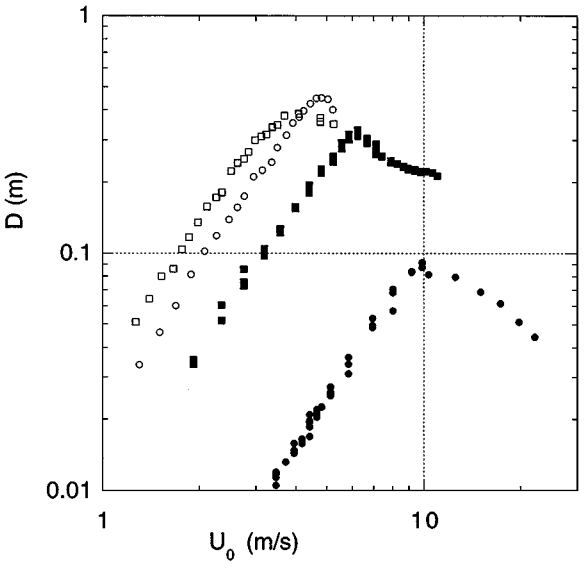

FIG. 5. Diameter of a water sheet as a function of jet velocity. The jet diameters were 0.8 (filled circles), 2.8 (filled squares), 4 (open circles), and 5 mm (open squares).

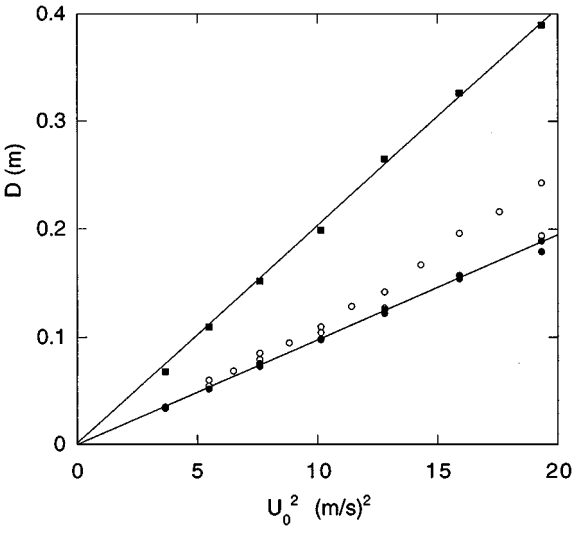

FIG. 7. Diameter of the same sheet as before, but as a function of the square of the jet velocity and in a linear scale to point out the transition occurring with the 1% Ajax solution.

tension forces. The rim then fragments into dispersed droplets, which detach from the liquid sheet (Fig. 8).

The position of the quasi-stationary rim is given by an equilibrium between the incoming liquid momentum flux and the surface tension forces which pull the rim toward the center. If $e(r)$ is the sheet thickness and $u(r)$ the sheet velocity at radial location r from the axis, the equilibrium at the rim of position $r = R$ may be written as

$$\rho e(R)u^2(R) = 2\sigma, \qquad [1]$$

where σ is the surface tension at the rim and ρ is the density of the liquid. This relation also provides the recession velocity of the rim of a stationary film. Its validity has been established in several liquid film experiments (12–14).

In a first analysis, we will derive the liquid velocity and sheet thickness for a plane sheet, neglecting viscous friction on the disk. The velocity of the liquid in the sheet, assumed to be uniform on a section, depends on the jet velocity u_0, the jet diameter d_0, and the height of fall h_0.

For mass, momentum, and kinetic energy conservation, we choose a steady control volume V of surface S delimited by the nozzle exit and a distance r from the axis, where sheet thickness is $e(r)$. Mass M conservation on this volume, $dM/dt = 0$, implies that the sum of the incoming flux of mass is zero, since flow is stationary in the volume:

$$\oint_S \rho \mathbf{u} \cdot \mathbf{n}\, ds = 0. \qquad [2]$$

This implies

$$\frac{\pi}{4} d_0^2 \rho u_0 = 2\pi r e(r) \rho u(r). \qquad [3]$$

According to Bernoulli's theorem applied on a stream line for stationary flow

$$\frac{1}{2}\rho u^2 = \frac{1}{2}\rho u_0^2 + \rho g h_0 + \frac{2\sigma}{d_0}. \qquad [4]$$

The magnitude of the pressure due to height of fall $\rho g h_0$ and of internal pressure due to surface tension $2\sigma/d_0$ is small $[((2\sigma/d_0)/\rho u_0^2/2) < 0.04$ and the nozzle exit was as close as possible from the impingement surface so that $\rho g h_0/(\rho u_0^2/2) \ll 1]$. Then from Eq. [4] we have $u(r) \simeq u_0$ in the inviscid limit. The fluid velocity is constant in the sheet: considering a small volume element of the liquid sheet, its surface increases as it is

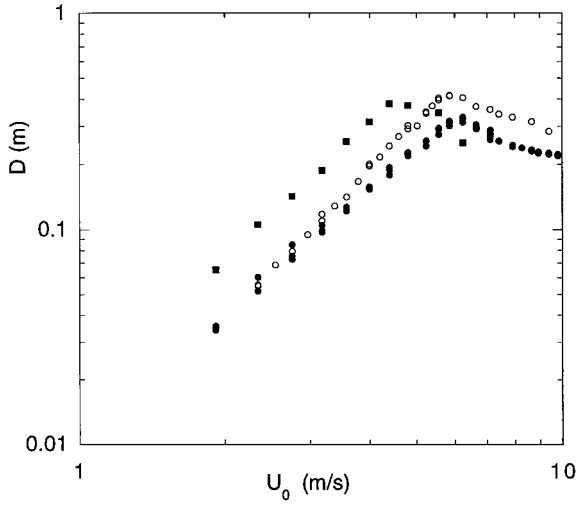

FIG. 6. Diameter of the sheet as a function of jet velocity for different surfactant concentrations of Ajax. Filled circles, pure water; open circles 1% (in volume) Ajax solution; squares, 20% Ajax solution.

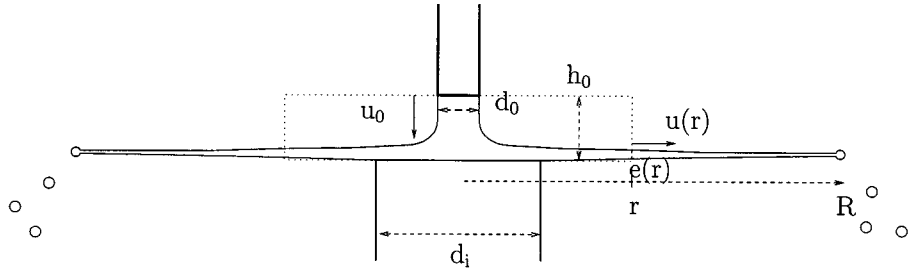

FIG. 8. Impact on the disk. Dots: control volume V.

convected toward the rim, but the net capillary force acting on it is zero and therefore its kinetic energy is constant.

The sheet thickness derives from mass conservation (Eq. [3]) and we have the two main results of the inviscid analysis of the flow:

$$u(r) = u_0, \qquad [5]$$

$$e(r) = \frac{d_0^2}{8r}. \qquad [6]$$

The rim is motionless at the equilibrium position $R = D/2$ derived from Eq. [1]:

$$\frac{D}{d_0} = \frac{1}{8}\frac{\rho u_0^2 d_0}{\sigma} = \frac{We}{8}, \qquad [7]$$

where $We = \rho u_0^2/(\sigma/d_0)$ is the Weber number, expressing the ratio of inertial forces to surface tension forces. We do not address the problem of the stability of the rim here. The important point to note at this stage is that corrugations of the rim and the subsequent drop formation process have an amplitude much smaller than the average radius of the sheet (Fig. 4), so that D in Eq. [7] is actually a well-defined quantity.

4.2. *Influence of Viscosity*

We have until now neglected any viscous dissipation. We will therefore estimate the effect of viscous friction on the impacting disk of diameter d_i. The kinetic energy balance between nozzle exit and a position r in the sheet (with r larger than the radius of the disk $d_i/2$) is modified, including the power dissipated by friction on the whole disk:

$$\oint_S \frac{1}{2}\rho u^2 \mathbf{u}\cdot\mathbf{n}\, ds = -\int_V \frac{1}{2}\rho\nu\left(\frac{\partial u}{\partial z}\right)^2 dv, \qquad [8]$$

where ν is the kinematic viscosity of the liquid. Considering that $\partial u/\partial z$ is of order $\frac{u}{\delta}$, with δ the boundary layer thickness, we obtain

$$\frac{1}{2}\rho u^2 u 2\pi r e - \frac{1}{2}\rho u_0^2 u_0 \frac{\pi d_0^2}{4} = -\alpha\rho\nu\left(\frac{u}{\delta}\right)^2 \delta\frac{\pi d_i^2}{4}. \qquad [9]$$

The last term comes from dimensional analysis, and α is a geometrical factor ($\alpha \simeq 1$). The boundary layer thickness is $\delta \sim (\nu d_i/u_0)^{1/2}$ at the disk edge. With the unchanged mass conservation, the velocity of the liquid after friction on the disk may be written as a function of the initial velocity and the Reynolds number of the flow:

$$u = \frac{u_0}{\left(1 + 2\alpha\frac{(d_i/d_0)^{3/2}}{\sqrt{Re}}\right)^{1/2}} = \beta u_0, \qquad [10]$$

$$Re = \frac{u_0 d_0}{\nu}, \qquad [11]$$

where β is a correction factor ($0 < \beta < 1$) depending weakly on the initial Reynolds number. The sheet thickness is $e(r) = d_0^2/(8\beta r)$, and the radius of the sheet is then given by

$$\frac{D}{d_0} = \frac{1}{\left(1 + 2\alpha\frac{(d_i/d_0)^{3/2}}{\sqrt{Re}}\right)^{1/2}}\frac{We}{8} = \beta\frac{We}{8}. \qquad [12]$$

Equation [12] corresponds to the inviscid equation [7] corrected by a factor β function of Re, and of order unity in practice.

4.3. *Conical Sheet*

When the sheet expands in a conical shape, if, for instance, the ring of the impactor is pulled higher, gravity has to be taken into account. The Bernoulli relation for an inviscid fluid, applied between the impacting disk edge and the sheet rim of height h, provides

$$\frac{1}{2}u^2 = \frac{1}{2}u_h^2 + gh. \qquad [13]$$

Mass conservation gives the thickness of the sheet, and the equality of the recession and liquid velocity gives the length of the cone:

$$L = \frac{1}{16}\beta We(1 - 2gh/u^2)^{1/2}. \qquad [14]$$

The radius $R = D/2$ of the base of the cone and the height h of the cone are related to its length by $R^2 + h^2 = L^2$. Then

$$\sqrt{\frac{R^2 + h^2}{1 - 2gh/u^2}} = \frac{1}{16}\beta We. \qquad [15]$$

The corrected radius $R_{corr} = [(R^2 + h^2)/(1 - 2gh/u^2)]^{1/2} \simeq [(R^2 + h^2)/(1 - 2gh/u_0^2)]^{1/2}$ follows the same law as the radius of the flat sheet.

4.4. Comparison with the Water Experiments

The nondimensional sheet diameter D/d_0 versus the injection Weber number $We = \rho u_0^2 d_0/\sigma$ is plotted in Fig. 9, with $\rho = 1000$ kg/m^3 and $\sigma_{\text{water}} = 70$ mN/m. For the 4- and 4.9-mm jets, the sheet was conical and we plotted the corrected diameter (see Eq. [15]).

The sheet diameter is fairly proportional to the Weber number until the latter reaches the value of 1000; then it decreases because of the development of a shear instability with the air [see, e.g., (11)]. We will not describe the instability here, but we emphasize that this phenomenon, occurring for large liquid velocities, restricts the range of observation for which Eq. [12] holds.

In the viscous prediction of the diameter, we found a correcting factor β depending on α, an unknown geometrical factor. To match experimental data, this factor α has to be equal to 1.5, 3.9, 4.1, and 2.0 for jet diameters of 0.8, 2.9, 4.0, and 4.9 mm, respectively. The prefactors α are somewhat different from case to case because of the different shapes and convergence ratio of the injector nozzles.

5. ADSORPTION KINETICS AT A STRETCHED INTERFACE

5.1. Diffusion-Controlled Model

This experiment allows the adsorption at the surface of a surfactant dissolved in a liquid to be monitored. There is indeed a continuous creation of a fresh surface, stretched in the radial flow. The surface is gradually repopulated by surfactant molecules, and this causes the surface tension to decrease with respect to the pure water value. The surface tension at the rim is therefore lower than with pure water, and the radius of the circular sheet is larger, since, according to Eq. [12], it is inversely proportional to the surface tension at the rim.

We assumed that the top and bottom surfaces of the liquid sheet have the same surface tension at the rim, the surface being extremely expanded and the initial difference of adsorption (the top surface is created before the bottom) being negligible, as we will quantitatively show below.

The amount of surfactant Γ adsorbed at the surface is related to the surface pressure $\Pi = \sigma_{\text{water}} - \sigma$ by the Frumkin equation of state, which assumes a monolayer of localized and interaction free molecules (15):

$$\Pi = -RT\Gamma_\infty \ln(1 - \Gamma/\Gamma_\infty), \qquad [16]$$

where R is the ideal gas constant, T is the temperature, and Γ_∞ (in mol m^{-2}) is the maximum surface concentration.

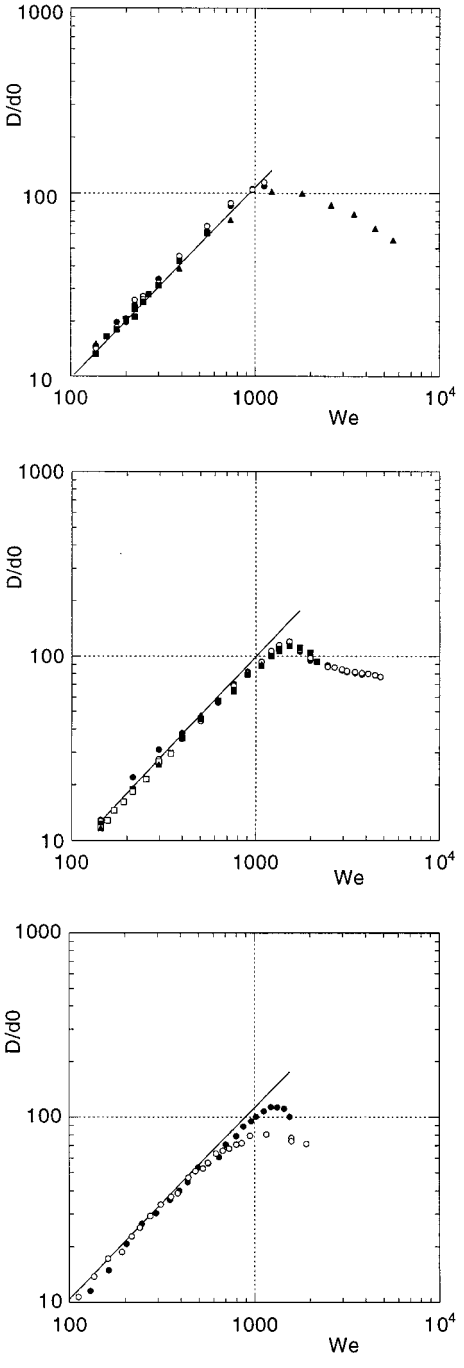

FIG. 9. Liquid sheet diameter D as a function of the injection Weber number $We = \rho u_0^2 d_0/\sigma$: top, jet diameter is 0.8 mm; middle, jet diameter is 2.8 mm; bottom, jet diameters are 4 (filled circles) and 4.9 mm (open circles). Symbols: different experimental data. Solid line: prediction including viscosity.

What can we expect for the adsorption kinetics? There are two steps in the process of adsorption: diffusion of surfactant from bulk toward the subsurface volume and then the transfer from subsurface to surface. We studied surfactants whose adsorption is controlled by diffusion. In this case, diffusion through the solution was the limiting step, transfer at the interface being far quicker. Bleys and Joos (16) tabulate the ratio $\mathcal{R} = \tau_D/\tau_K$ of the characteristic diffusion time $\tau_D = (d\Gamma/dC)^2/D$ and the characteristic transfer time $\tau_K = k^{-1}$, inverse of the transfer rate, for a panel of surfactants. At low concentrations, $\mathcal{R}$ is found to be 131 for octan-1-ol.

The concentration of surfactant on an axis Oz perpendicular to the surface and oriented toward the liquid is $C(z, t)$. In the diffusion-controlling limit, an equilibrium between adsorption $\Gamma(t)$ and subsurface concentration $C(z = 0, t)$ is reached at all times, given by a Langmuir isotherm:

$$\Gamma(t) = \Gamma_\infty \frac{C(0,t)}{C(0,t) + a}, \qquad [17]$$

where a is the Langmuir–Von Szyszkowski coefficient.

The evolution of Γ is given by Fick's law, for a diffusion coefficient D:

$$\frac{d\Gamma}{dt} + \Gamma\Theta = D\frac{\partial C}{\partial z}(0,t), \qquad [18]$$

where $\Theta = (1/dS)(d/dt)\,dS$ is the dilatation rate of the surface, with dS a small surface moving with the liquid. A cylindrical element of volume $dV = \pi d_0^2 dx/4$ before impingement has a surface area $dS_0 = \pi d_0\,dx$. Stretched after impact, this volume becomes a ring whose top plus bottom area is $dS = 4\pi r\,dr$ (Fig. 10). The velocity in the sheet is constant and equal to β times the initial velocity, so that $dr = \beta\,dx$. At a radial position r in the sheet, the area of the elementary volume has thus been augmented by a factor

$$\frac{dS}{dS_0} = 4\beta\frac{r}{d_0}. \qquad [19]$$

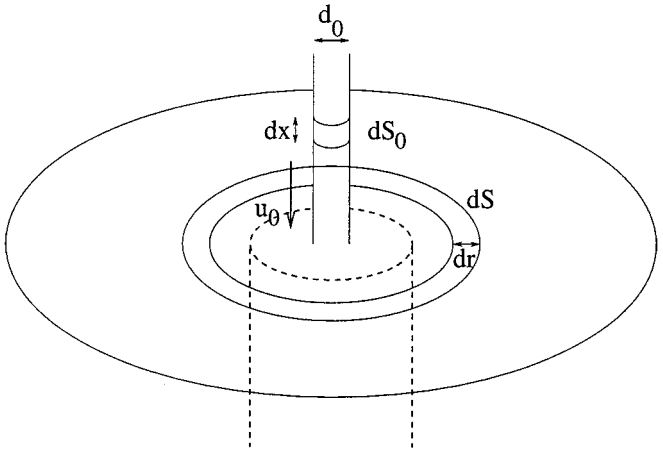

FIG. 10. Stretching of a small surface on the jet after impact.

At the rim, the surface area has been increased by a factor $4\beta R/d_0 = \beta^2 We/4$, ranging from 24 to 240 in our experiments.

Stretching begins when the jet impacts the disk, at radius $r = d_0/2$, and we consider a small surface dS located at this radius at time $t = 0$. The radial position of dS at time t is $r = ut + d_0/2$. Then, using Eq. [19], we have $dS = 2(ut/d_0 + 1/2)\beta\,dS_0$. The stretching rate is

$$\Theta = \frac{1}{t + d_0/2u} = \frac{1}{t + t_0}, \qquad [20]$$

where $t_0 = d_0/2u$ is the time for onset of stretching, which ranges from 0.2 to 2 ms in the present experiments. The diffusion equation is

$$\frac{\partial C}{\partial t} - \Theta z\frac{\partial C}{\partial z} = D\frac{\partial^2 C}{\partial z^2}, \qquad [21]$$

because in the frame of the moving liquid, the thinning velocity of the sheet parallel Oz is $v_z = -\Theta z$. Diffusion takes place to a depth smaller than the liquid sheet thickness, so the top and bottom diffusion layers do not interfere, an assumption which we come back to below.

The boundary value problem is

$$\frac{\partial C}{\partial t} - \frac{z}{t + t_0}\frac{\partial C}{\partial z} = D\frac{\partial^2 C}{\partial z^2}, \qquad [22]$$

$$\frac{d\Gamma}{dt} + \frac{\Gamma}{t + t_0} = D\frac{\partial C}{\partial z}(0,t), \qquad [23]$$

$$C(z, 0) = C_0, \qquad [24]$$

$$\lim_{z\to\infty} C(z,t) = C_0. \qquad [25]$$

For a nonstretched interface ($\Theta = 0$ or $t_0 \to \infty$) with an initial volume concentration C_0, the solution of the diffusion equation was given by Ward and Tordai (4):

$$\Gamma(t) = \Gamma(0) + 2\left(\frac{D}{\pi}\right)^{1/2}\left\{C_0\sqrt{t} - \int_0^{\sqrt{t}} C(z=0, t-\lambda)d\sqrt{\lambda}\right\}. \qquad [26]$$

The problem including stretching is solved by introducing a new nondimensional variable $\xi = z/e(t)$ for the z coordinate that accounts for the fact that the sheet thickness is a function of time. To transform the convective diffusion equation [22] into a pure diffusion equation, we nondimensionalize time t to τ by

$$\xi = \frac{z}{e(t)} = \frac{4z}{d_0}(t/t_0 + 1), \qquad [27]$$

$$\tau = D\int_0^t \frac{dt'}{e(t')^2} = \frac{8}{3Pe}((t/t_0 + 1)^3 - 1), \qquad [28]$$

where Pe is the Péclet number, defined as $u_0 d_0/D$. With those

new variables, Eqs. [22] and [23] are transformed into

$$\frac{\partial C}{\partial \tau} = \frac{\partial^2 C}{\partial \xi^2}, \quad [29]$$

$$\frac{d}{d\tau}\left(\frac{4}{d_0}(t/t_0+1)\Gamma(t)\right) = \frac{\partial C}{\partial \xi}(0,\tau), \quad [30]$$

which are the classical diffusion equations solved by Ward and Tordai. We are now able to justify our above assumption of the independence of the top and bottom diffusive layers. According to Eq. [29], the diffusion layer is about $\delta/e \sim \sqrt{\tau}$. At the edge, the adsorption time is $t = R/u_0, t \gg t_0$. We have

$$\frac{\delta}{e} = \frac{1}{8\sqrt{3}}\frac{We^{3/2}}{Pe^{1/2}}. \quad [31]$$

In our experiments ($We < 1000$ and $Pe > 3.5 \times 10^7$), the value of δ/e given by Eq. [31] is always smaller than 0.4, so the top and bottom diffusive layers can be considered as independent.

The solution of the new set of equations [29] and [30] is, similarly to the Ward and Tordai solution,

$$\frac{4}{d_0}(t/t_0+1)\Gamma(t) = \frac{4}{d_0}\Gamma(0) + \frac{2}{\sqrt{\pi}}C_0\sqrt{\tau} - \frac{2}{\sqrt{\pi}}\int_0^{\sqrt{\tau}} C(z=0,\tau-\lambda)\,d\sqrt{\lambda}. \quad [32]$$

Assuming a clear initial surface ($\Gamma(0) = 0$), before the onset of stretching, the adsorption is the same as for a nonstretched interface according to Eq. [32]:

$$t \ll t_0 \quad \Gamma(t) \simeq 2C_0\sqrt{\frac{Dt}{\pi}}. \quad [33]$$

Then stretching comes into play and the evolution of adsorption is

$$t \gg t_0 \quad \Gamma(t) \simeq 2C_0\sqrt{\frac{Dt}{3\pi}}. \quad [34]$$

The evolution is three times slower than for a nonstretched interface. When accumulation of surfactant is high enough to feed backward diffusion, we have to take into account the last term of Eq. [32], and at long times, adsorption tends to its equilibrium value $\Gamma_{eq} = \Gamma(C_0)$. The characteristic diffusion time needed to reach equilibrium is obtained by extrapolation of Eq. [34] to $\Gamma = \Gamma_{eq}$:

$$t_D = \frac{3\pi}{4D}\left(\frac{\Gamma_{eq}}{C_0}\right)^2. \quad [35]$$

Adsorption $\Gamma = \Gamma_{eq}(3t/t_D)^{1/2}$ at times much smaller than t_0, and $\Gamma = \Gamma_{eq}(t/t_D)^{1/2}$ at times larger than t_0. The transition between the two regimes appears in Fig. 11, where we plot Γ/Γ_{eq} as a function of t/t_D. The duration of this transition is clear when we relate adsorption and time to their values at t_0 (see $\Gamma/\Gamma(t=t_0)$ versus t/t_0 in Fig. 11). The transition begins at about $t = 0.1t_0$ and lasts until about $10t_0$. Afterward backward diffusion comes into play, adsorption reaches equilibrium. In the experiments, t_0 ranges from 0.2 to 2 ms, and our observation times, ranging from 10 to 100 ms, are larger.

The term due to surface adsorption accumulated before impact $\Gamma(0)$ fades away quickly. It is $\Gamma(0)/\{1+(\sigma_{\text{water}}/\sigma_{\text{rim}})We/8\}$ at the rim, and in our experiment we have $1/\{1+(\sigma_{\text{water}}/\sigma_{\text{rim}})We/8\} < 0.08$. Moreover, transit times on the sheet are larger than the transit time on the jet before impact (its order of magnitude is d_0/u_0 smaller than 3 ms in our experiments); the contribution of adsorption before impact is thus negligible.

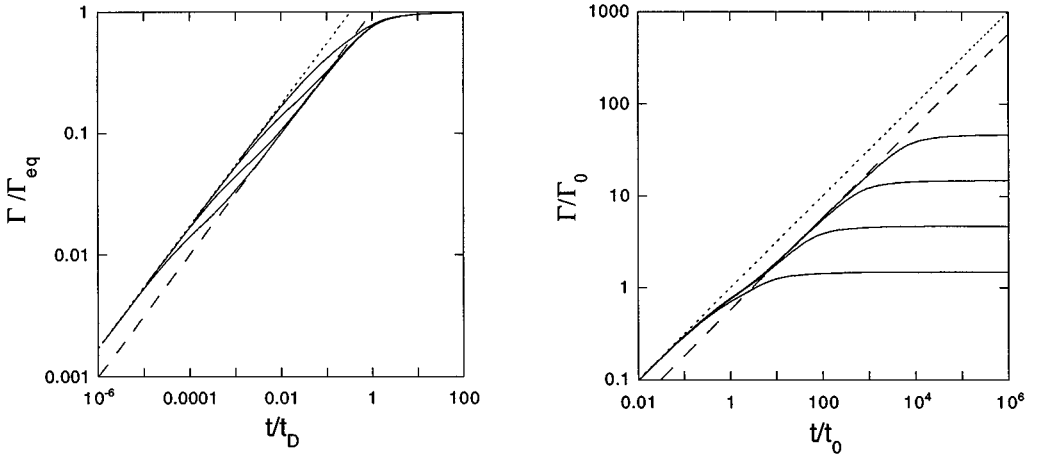

FIG. 11. Left: Ratio of adsorption to equilibrium adsorption Γ/Γ_{eq} versus time over characteristic diffusion time t_D for $t_0 = 10^{-2}, 10^{-3}, 10^{-4}$, and 10^{-5} s (solid lines, from top to bottom), without stretching (dotted line), and without stretching but with the time evolving three times slower (dashed line). Right: Ratio of adsorption Γ to adsorption $\Gamma_0 = \Gamma(t = t_0)$ for $t_0 = 10^{-2}, 10^{-3}, 10^{-4}$, and 10^{-5} s (solid lines, from bottom to top). Surfactant properties are $\Gamma_\infty = 6 \times 10^{-6}$ mol/m^2, $a = 2.4 \times 10^{-4}$, $C_0 = 1.4 \times 10^{-3}$ mol/L, and $D = 3.5 \times 10^{-10}$ m^2 s^{-1}.

The subsurface concentration $C(z = 0, t)$ needed in the integral of Eq. [32] is given by the Langmuir isotherm (Eq. [17]). These two equations are self-sufficient to compute the adsorption Γ numerically, and thus the surface tension σ as a function of time.

5.2. Determination of Dynamic Surface Tension

We have seen that for pure water the diameter of the sheet depends on the surface tension at the rim according to $D/d_0 = \beta\rho u_0^2 d_0/\sigma_{\text{rim}}$. In the presence of surfactants, surface tension decreases from the jet exit until the rim. If we neglect the Marangoni stress that arises from the variation of surface tension along the film, which will be justified later, film velocity is unchanged and the above relation is still valid. Then the sheet diameter reflects surface tension.

We can now understand the curves of Fig. 6. With the 20% solution, the interface is fully saturated at any velocity and surface tension has an equilibrium value of 27.8 mN/m (see static measurements below); the diameter is proportional to velocity squared. With the 1% solution, the interface is not fully saturated at the rim, but is increasingly saturated when injection velocity grows, because the sheet diameter is proportional to the square of velocity and therefore the transit time R_{eq}/u is proportional to velocity, whereas the characteristic diffusion time t_D is independent of velocity. The surface tension starting from that of water decreases toward its equilibrium value of 29.5 mN/m. This is the reason why sheet diameter starts close to the water line and then departs from it to reach a theoretical line corresponding to the saturated surface tension 29.5 mN/m.

We deduce the rim surface tension from Eq. [12] as a function of the measured diameter D of the sheet and the injection velocity u_0:

$$\sigma_{\text{rim}} = \frac{\rho u_0^2 d_0^2}{8\beta D}. \qquad [36]$$

The transit time of the surface since its creation until it reaches the rim is simply

$$t = \frac{D}{2\beta u_0}. \qquad [37]$$

We have neglected the fact that the sheet velocity is intermediate between u_0 and u during friction on the disk, because the disk diameter is small compared to the measured sheet diameters.

The experimental surface tension versus time curve is thus obtained; it will allow us to compare measurements with our model of adsorption kinetics for different surfactants. The minimum transit time we measured, corresponding to the smallest sheet we could produce with the smallest nozzle diameter we used (2.75 mm), was 10 ms. The surface tension versus diameter relation is valid for a stable sheet only. With the bigger nozzle diameters we used (5 mm), the sheet was stable for a maximum transit time of 100 ms.

5.3. Radial Gradient of Surface Tension: Marangoni Stresses

We have up to now neglected any radial stress on the film due to the variation of surface tension. To estimate the impact of Marangoni stress on the flow, we will consider a small element of the film of volume $dV = e(r)dr\, r\, d\theta$ in cylindrical coordinates. The intensity of Marangoni forces on its top and bottom faces is $2(\partial\sigma/\partial r)dr\, r\, d\theta$. We assume a flat velocity profile in the film. If Marangoni stresses initially create a shear layer on the two faces of the film, the time of growth of this shear layer across the film is short compared to the transit time: it is of order e^2/ν_1, always smaller than 10 ms (sheet thickness at the rim being smaller than 0.1 mm according to Eqs. [6] and [7]), which is our minimum transit time. Hence the homogeneity of velocity in the film is a reasonable approximation. Momentum conservation then provides the evolution of film velocity u:

$$\rho e(r)\frac{du}{dt} = 2\frac{\partial\sigma}{\partial r}. \qquad [38]$$

Using the fact that the surface tension gradient is related to surface tension decrease by $\partial\sigma/\partial r = (\partial\sigma/\partial t)/u$ and that the derivative of σ with time is negative, we see that velocity decreases. To simplify the resolution of this equation, we will assume that the surface tension decrease remains constant, while it diminishes from an initial value as time elapses, as observed on experimental data. Then the integration of Eq. [38] gives a lower limit of the drop of the velocity u_M at the rim for all times:

$$\frac{u_M}{u_0} \geq \left(1 - \frac{3}{4}\frac{\Delta\sigma}{\sigma}\right)^{1/3}, \qquad [39]$$

where $\Delta\sigma = \sigma_{\text{water}} - \sigma$. The film velocity drop is zero initially and then increases when surface tension decreases. The estimation of the maximum error on velocity we made neglecting Marangoni stresses is given by the maximum surface tension drop on the approximately linear part of the surface tension versus time curves (Table 1).

The resulting slowing down of the liquid, which implies an underestimation of surface tension and transit time on the same proportion (see Eqs. [36] and [37]), is significant for high Ajax concentrations and at large times only.

TABLE 1
Effect of Marangoni Stress on Film Velocity

Solution	Maximum surface tension drop (mN/m)	Velocity drop $(u_0 - u_M)/u_0$
1.4×10^{-3} mol/L octanol	15	7.3×10^{-2}
2.5×10^{-3} mol/L octanol	20	11×10^{-2}
1% Ajax	15	7.3×10^{-2}
20% Ajax	30	24×10^{-2}

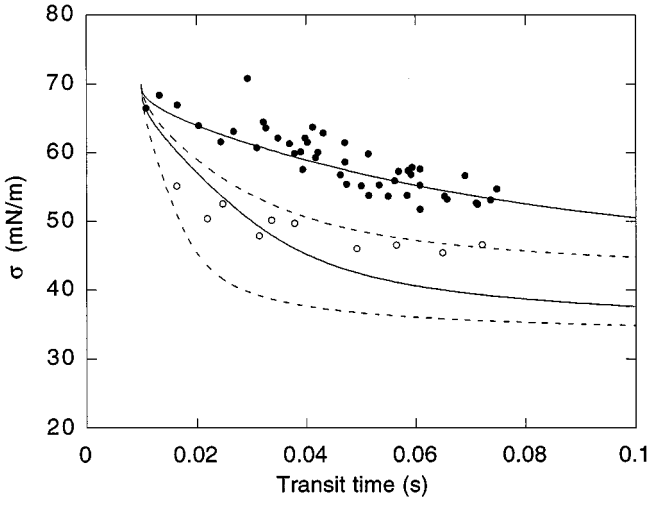

FIG. 12. Octan-1-ol solution surface tension versus time at concentrations of 1.4×10^{-3} (filled symbols) and 2.5×10^{-3} mol/L (open symbols). Lines, predictions of diffusion theory with stretching of interface for 1.4×10^{-3} and 2.5×10^{-3} mol/L; dashed lines, prediction without stretching. The diffusion coefficient used in calculation is $D = 5 \times 10^{-10}$ m^2 s^{-1}. We obtain a better fit by introducing a 10-ms delay (time for transfer from subsurface to surface).

5.4. Octan-1-ol

We first experimented with decanoic acid: its adsorption kinetics is too rapid and cannot be observed within the observation range allowed by our setup. The measured surface tensions were static values. Octan-1-ol and Ajax displayed the transition between a clean interface and a saturated interface.

Many kinetic experiments have been dedicated to octan-1-ol (5, 7, 15, 16), and it appears to be diffusion controlled. Its Langmuir isotherm parameters are experimentally found to be $\Gamma_\infty = 6 \times 10^{-6}$ mol/m^2 and $a = 2.1 \times 10^{-4}$ mol/L.

Experimental points and predictions are shown in Fig. 12, for 1.4×10^{-3} and 2.5×10^{-3} mol/L concentrations, with a best-fitting diffusion coefficient $D = 5 \times 10^{-10}$ m^2 s^{-1}. For comparison, we plotted the prediction for a nonstretched interface according to Eq. [32], and it is far too low compared with measurements. The agreement is not so good for high concentrations, possibly because of evaporation of the surfactant for big diameters. Nondimensional adsorptions are plotted in Fig. 13; they feature the same initial behavior (adsorption is growing at a rate proportional (time)$^{1/2}$) and then surface saturation slows down adsorption growth, sooner for the larger surfactant concentration.

We observe that a time delay of 10 ms better fits the data. This can be explained by Hansen's hypothesis (18) of a small adsorption barrier, developed to account for the fact that the decrease of surface tension does not exhibit an infinite slope initially, i.e., no infinite flux of adsorption, contrary to what is predicted by a pure diffusion-controlled model. The transfer process limits the initial adsorption for times shorter than the inverse of the transfer kinetics constant k. In this view, the delay time would correspond to the time necessary to establish equilibrium between subsurface bulk and surface. Then diffusion controls the kinetics because its time scale becomes larger, as shown by the agreement between experiment and predictions based on a pure diffusion mechanism. The transfer kinetics is well accounted for by Langmuir kinetics: $d\Gamma/dt = k(\Gamma_{eq}(C_s) - \Gamma)$, where $\Gamma_{eq}(C_s)$ is the equilibrium adsorption corresponding to the local subsurface bulk concentration $C_s = C(0, t)$ with the Langmuir adsorption isotherm 17. For octan-1-ol, the rate constant is assumed to be $k = 200$ s^{-1} in the small-concentration limit by Bleys and Joos (16), which provides a characteristic time of 5 ms comparable in order of magnitude to our delay time.

5.5. Industrial Detergent

To find out the Ajax adsorption parameters Γ_∞ and a, static surface tension measurements were made for different concentrations of surfactant (Fig. 14). The surface tension decreases with concentration until it reaches the critical micellar concentration (cmc $\simeq 5 \times 10^{-3}$ L/L), above which the greatest part of additional surfactant goes into micelles. Ajax does not include a lot of insoluble surfactant impurities; otherwise the positive growth at the cmc would have been more important, because insoluble surfactant tends to go in the micelles, where it is protected against water.

The static surface pressure Π below the cmc comes from the Frumkin equation of state (Eq. [16]) and equilibrium between the surface and subsurface (Eq. [17]):

$$\Pi = RT\Gamma_\infty \ln\left(1 + \frac{c}{a}\right). \qquad [40]$$

This parameter allows computation of the evolution of surface tension with time.

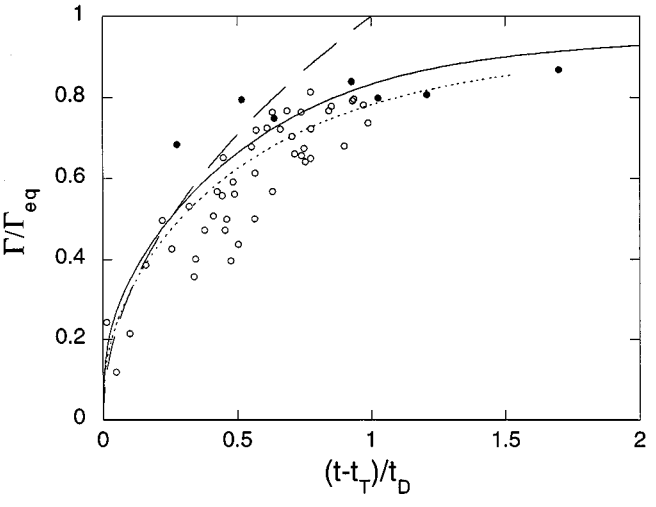

FIG. 13. Nondimensional adsorption of octan-1-ol solutions versus time (minus a delay time $t_T = 10$ ms) divided by characteristic adsorption time t_D for concentrations of 1.4×10^{-3} (filled symbols) and 2.5×10^{-3} mol/L (open symbols). Lines, predictions of diffusion theory with stretching of interface for 1.4×10^{-3} and 2.5×10^{-3} mol/L (dotted); dashed line, $((t - t_T)/t_D)^{1/2}$.

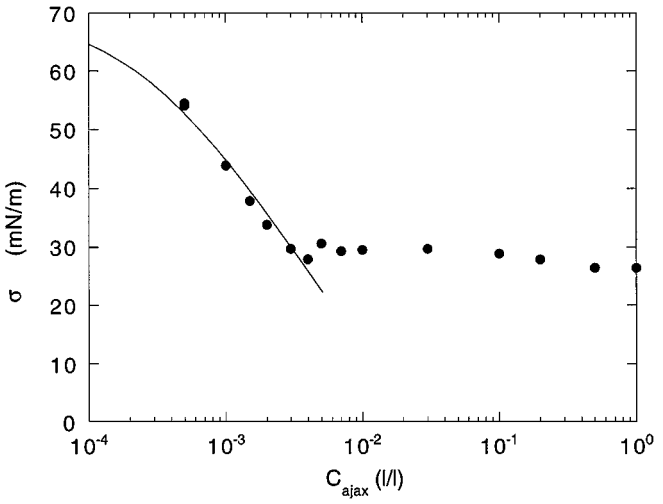

FIG. 14. Static surface tension of Ajax solution versus Ajax volume concentration: circles, measures; line, Frumkin equation of state, with $\Gamma_\infty = 6.2 \times 10^{-6}$ mol/m^2 and $a = 2.4 \times 10^{-4}$.

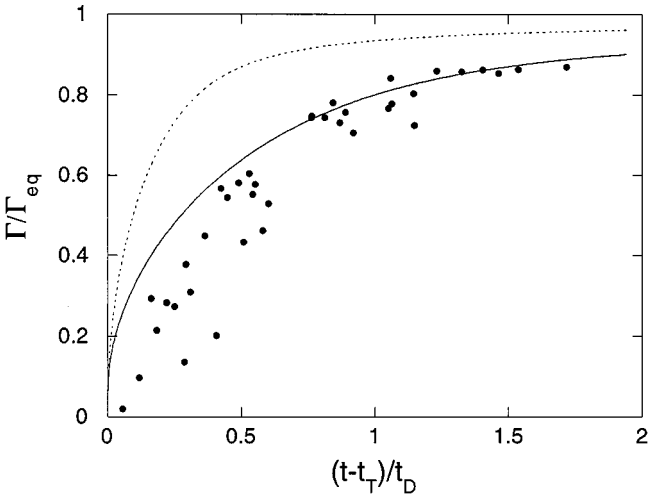

FIG. 16. Nondimensional adsorption of an Ajax solution versus time (minus a delay time $t_T = 10$ ms) divided by characteristic adsorption time t_D; volume concentration is 1%. Lines, predictions for diffusion theory with stretching of interface; dotted line, without stretching.

For dynamic experiments with the liquid sheet, we have chosen concentrations above the cmc. In this case, relation [40] is not valid because of the presence of micelles. For a rough estimate, we assumed the relation to be still valid and chose for computation concentrations giving the same static surface tension drop (2×10^{-3} and 3.5×10^{-3} L/L instead of 1 and 20%). We do not know the molar concentration n_0 of pure Ajax, which is necessary to link molar concentration C_0 to volumic concentration C_v with $C_0 = n_0 C_v$. However, the quantity necessary to compute adsorption is $C_0 D^{1/2} = C_v (n_0^2 D)^{1/2}$ (see Eq. [26]), so we will fit the model with $n_0^2 D$ instead of D as we did with octanol.

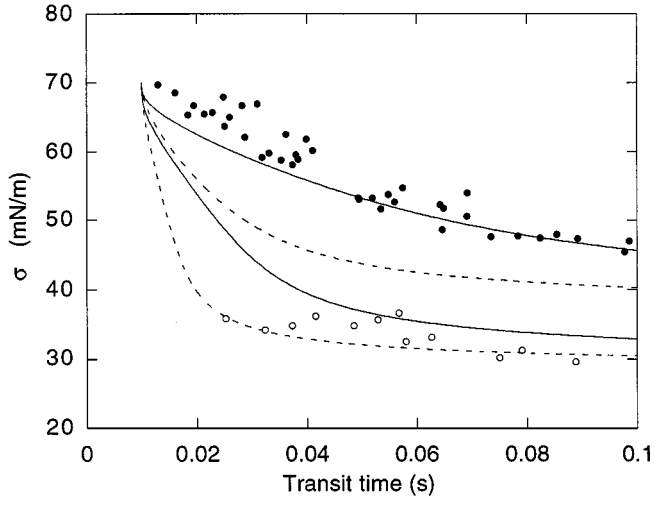

FIG. 15. Ajax solution surface tension versus time; volume concentrations of 1 (filled symbols) and 20% (open symbols). Lines, predictions of diffusion theory with stretching of interface for 1 and 20%; dotted lines, prediction without stretching. We obtain a better fit by introducing a 10-ms delay (time for transfer from subsurface to surface).

Experimental and theoretical results are plotted in Fig. 15 for surface tension and in Fig. 16 for nondimensional adsorption. The diffusion coefficient is $n_0^2 D = 3.5 \times 10^{-10}$ mol^2 L^{-2} m^2 s^{-1}. As with octanol, a 10-ms time delay is introduced that accounts for the initially controlling transfer process.

6. SUMMARY

The diameter of the thin liquid sheet formed by the impact of a jet was studied with pure water and found to be a function of jet velocity and surface tension at the rim. The friction on the disk is accounted for by a dimensional estimation and provides a way to predict the sheet diameter for each jet and impactor diameters.

We used these results to derive the surface tension at the rim of the sheet from measurements of its diameter. We have shown that the liquid sheet diameter is fixed by a competition between stretching-induced surface creation and diffusion-controlled repopulation of the interface by dissolved surfactants. Experimental measurements of surface tension are accurate enough to observe a diffusion-controlled kinetics of adsorption.

This experimental setup thus allows due to visualize quantitatively the impact of adsorption kinetics on surface tension by the simple measurement of a macroscopic length (the sheet diameter) in a stationary flow. It provides a new method to monitor adsorption in the time range 10–100 ms.

ACKNOWLEDGMENTS

This work was financially supported by the Société Européenne de Propulsion (SEP) under Contract 910023 via the GDR Combustion dans les moteurs de fusées. A. Cartellier and L. Davoust are gratefully acknowledged for their advice.

REFERENCES

1. Dupré, A., "Théorie mécanique de la chaleur." Gauthier-Villars, Paris, 1869.
2. Rayleigh, J. W. S., *Proc. R. Soc. London, Ser. A* **71,** 29 (1879).
3. Bond, W. N., and Puls, H. O., *Philos. Mag.* **24,** 864 (1937).
4. Ward, A. F. H., and Tordai, L., *J. Chem. Phys.* **14,** 453 (1946).
5. Defay, R., and Hommelen, J. R., *J. Colloid Sci.* **13,** 553 (1958).
6. Defay, R., and Hommelen, J. R., *J. Colloid Sci.* **14,** 411 (1959).
7. Joos, P., Bleys, G., and Petré, G., *J. Chim. Phys.* **79,** 387 (1982).
8. Savart, F., *Ann. Chim. Phys.* **LIX,** 55, 113 (1833).
9. Harkins, W. D., and Brown, F. E., *J. Am. Chem. Soc.* **41,** 499 (1919).
10. Wilkinson, M. C., *J. Colloid Interface Sci.* **40,** 14 (1972).
11. Huang, J. C. P., *J. Fluid Mech.* **43,** 305 (1970).
12. Ranz, W. E., *J. Appl. Phys.* **30,** 1950 (1959).
13. McEntee, W. R., and Mysels, K. J., *J. Phys. Chem.* **73,** 3018 (1969).
14. Pandit, A. B., and Davidson, J. F., *J. Fluid Mech.* **212,** 11 (1990).
15. Fowler, R., and Guggenheim, E. A., "Statistical Thermodynamics." Cambridge Univ. Press, Cambridge, UK, 1952.
16. Bleys, G., and Joos, P., *J. Phys. Chem.* **89,** 1027 (1985).
17. Posner, A. M., Anderson, J. R., and Alexander, A. E., *J. Colloid Sci.* **7,** 623 (1952).
18. Hansen, R. S., *J. Colloid Sci.* **16,** 549 (1961).